Numerical investigation of aerodynamic performance of darrieus wind turbine based on the magnus effect

Lahouari Khadir[1] and Hatem Mrad[2, *]
[1]University of Science and Technology of Oran - Mohamed-Boudiaf, BP 1505, Bir El Djir 31000, Algeria
[2]School of Engineering, University of Quebec at Abitibi-Timiscamengue, Rouyn-Noranda, J9X 5E4, Canada

ABSTRACT

The use of several developmental approaches is the researchers' major preoccupation with the DARRIEUS wind turbine. This paper presents the first approach and results of a wide computational investigation on the aerodynamics of a vertical axis DARRIEUS wind turbine based on the MAGNUS effect. Consequently, wind tunnel tests were carried out to ascertain overall performance of the turbine and two-dimensional unsteady computational fluid dynamics (CFD) models were generated to help understand the aerodynamics of this new performance. Accordingly, a moving mesh technique was used where the geometry of the turbine blade was cylinders. The turbine model was created in Gambit modeling software and then read into fluent software for fluid flow analysis. Flow field characteristics are investigated for several values of tip speed ratio (TSR), in this case we generated a new rotational speed ratio between the turbine and cylinder ($\delta = \omega_C/\omega_T$). This new concept based on the MAGNUS approach provides the best configuration for better power coefficient values. The positive results of Cp obtained in this study are used to generate energy; on the other hand, the negative values of Cp could be used in order to supply the engines with energy.

Keywords: Simulation, VAWT, MAGNUS Effect, Wind turbine

NOMENCLATURE

A [m^2]	Rotor swept area
C_N [–]	Wind turbine normal force coefficient
C_T [–]	Wind turbine thrust force coefficient
$C_{P,\,ave}$ [–]	Wind turbine power coefficient
$C_Q(\theta)$ [–]	Rotor instantaneous torque coefficient
$D_{cylinder}$ [mm]	Cylinder diameter
D_{rotor} [mm]	Rotor diameter
F_r [N]	Aerodynamic radial force
H_{rotor} [mm]	Rotor height
H_{domain} [mm]	Wind tunnel height

*Corresponding Author: E-mail: hatem.mrad@uqat.ca

$M(\theta)$ $[N.m]$	Rotor instantaneous torque
N	Number of cylinders
P_T $[W]$	Power available in wind
P_W $[W]$	Power produced by the wind turbine
R_e	Reynolds number
R $[mm]$	Rotor radius
u_T $[m/s]$	Tangential wall velocity
$V_{test\ section}$ $[m/s]$	Wind velocity at rotor test section
T $[N.m]$	Wind turbine torque output
$T.S.R$ [–]	Turbine tip speed ratio
U_∞ $[m/s]$	Free wind velocity
W_{domain} $[mm]$	Computational domain width
y $[mm]$	Wall-grid centroïd distance
y^+ [–]	Cylinder *y-plus*
ε_{sb} [–]	Solid blockage
δ [–]	Rotational speed ratio (turbine / cylinder)
Γ [m/s^2]	Circulation of a perfect fluid
θ [°]	Azimuthal position
λ [–]	Cylinder tip speed ratio
μ $[Pa.s]$	Dynamic viscosity
ρ $[kg/m^3]$	Air density
σ [–]	Rotor solidity
ω_T $[rad/s]$	Rotor (turbine) angular velocity
ω_C $[rad/s]$	Cylinder angular velocity

1. INTRODUCTION

First, Templin [1] developed a blade element-momentum single streamtube numerical model to predict the performance of a VAWT. Then, Strickland [2, 3] developed a blade element-momentum multiple streamtube numerical model to predict the performance of a VAWT rotor.

Paraschivoiu [4–7] developed analytical and numerical aerodynamic models to investigate the performance of VAWT, focusing on the phenomenon of dynamic stall. Mertens [8] developed a blade element-momentum multiple streamtube model to predict the performances of fast rotating VAWT in the skewed flow on a roof. As pointed out by Ferreira [9], the VAWT has an inherent unsteady aerodynamic behavior due to the variation of the angle of attack with the azimuthal position, of the relative velocity and, consequentially, of the Reynolds number. Wang and Tao [10] performed numerical simulations using a RANS model, by solving the Navier-Stokes equations with two low Reynolds number turbulence models. There are many experimental and numerical studies concerning the flow through Savonius rotor [11–13].

The Darrieus wind turbine was patented by the U.S. Patent Office in the name of G.J.M. Darrieus in 1931 [14]. The DARRIEUS-MAGNUS configuration showed in Figure 1 was carried out as the first approach to figure out the best aerodynamic performance.

1.1. MAGNUS EFFECT

The Magnus effect or Magnus force is the phenomenon whereby a spinning object flying in a fluid creates a whirlpool of fluid around itself, and experiences a force perpendicular to the line of motion. The overall behaviour is similar to that around an airfoil with a circulation which is generated by the mechanical rotation, rather than by aerofoil action in Figure 2.

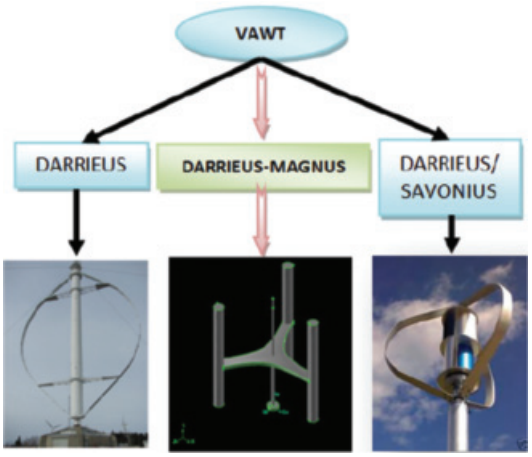

Figure 1: Different DARRIEUS wind turbines combination

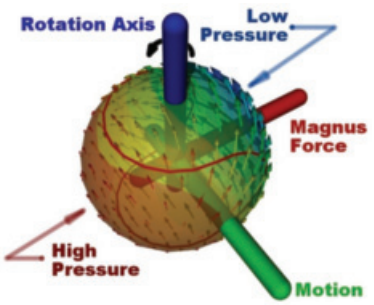

Figure 2: Magnus effect, around a cylinder in rotation

The Magnus effect is often considered a demonstration of Bernoulli's principle, but this is incorrect, as the viscosity of the air assumed to be negligible in Bernoulli's principle is central to understanding the magnitude of the force.

Considering the case of a perfect fluid, the equation of Bernoulli gives:

$$\frac{1}{2}\rho V_1^2 + P_1 = \frac{1}{2}\ \rho V_2^{\ 2} + P_2 \tag{1}$$

The speed difference between items (1) and (2) is thus at the origin of a pressure gradient between these two points:

$$P_2 - P_1 = \frac{1}{2}\rho\left(V_1^2 - V_2^2\right) = 2\rho\omega R V_0 \tag{2}$$

Where ω is a rotational speed, V_0 the fluid speed ad infinitum, and R the cylinder ray. Thus, this gradient of pressure generates a MAGNUS force.

Taking into account of the asymptotic theory of Moore (1957) [15], the circulation in the case of a perfect fluid can be written:

$$\Gamma = 2\ \pi V R = 2\pi\omega R^2 \tag{3}$$

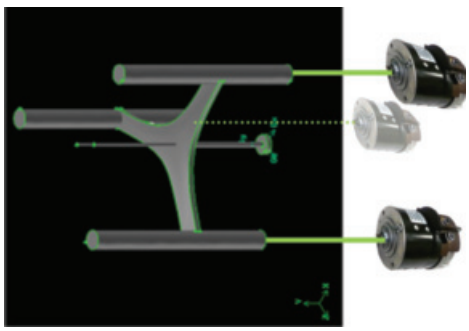

Figure 3: Engines integration for each cylinder

The theoretical lift coefficient for a perfect fluid is then given by:

$$C_{L_{pot}} = \frac{2\Gamma}{2V_0 R} = 2\ \pi \frac{\omega R}{V_0} = 2\pi\alpha \tag{4}$$

$\alpha = \omega R / V_0$ being the rate of rotation.

In this case, each cylinder could have appropriate power by using different engines as shown in Figure 3.

2. MODEL GEOMETRY

The aim of the present work was to numerically analyze the aerodynamic behavior of a 2D vertical-axis three-cylinder Darrieus wind turbine operating at different angular velocities ratios (δ) for a constant wind speed of 9 m/s.

The main features of the CFD simulation model are summarized in Table 1.

The cylinder azimuthal position was identified by the angular coordinate of the pressure of cylinder midsection, as can be seen in Figure 4.

3. SPATIAL DOMAIN DISCRETIZATION

As the aim of the present work was to reproduce the operation of a rotating machine, the use of moving sub-grids was necessary.

In particular, the discretization of the computational domain into macro-areas has led to two distinct sub-grids:

Table 1: Common features of the CFD simulation model

Blade profile	**Cylinder**
$D_{Cylinder}$ (mm)	85.8
D_{rotor} [mm]	1030
Hrotor [mm]	1456.4
A_s [m^2]	1.177
N [–]	3
$H_{wind\ tunnel}$ [mm]	4000
$W_{wind\ tunnel}$ [mm]	3800

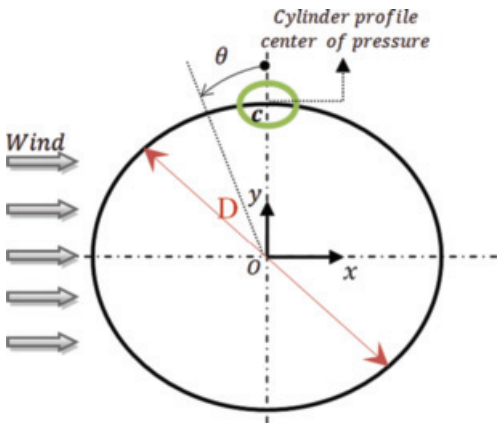

Figure 4: Cylinder azimuthal coordinate

A rectangular outer zone, determining the overall calculation domain, with a circular opening centered on the turbine rotational axis, which was identified as Wind Tunnel sub-grid, fixed.

A circular inner zone, which was identified as Rotor sub-grid, rotating with rotor angular velocity ω_T and cylinder angular velocity ω_c.

3.1. WIND TUNNEL SUB-GRID

Figure 5 shows the main dimensions and the boundary conditions of the Wind Tunnel sub-grid area.

Inlet and outlet boundary conditions were placed respectively 38 rotor diameters upwind and 62 diameters downwind with respect to rotor, allowing a full development of the wake, in accordance to what was suggested by the work of Ferreira et al. [16], who placed 10 test sections for a wind tunnel CFD simulation. Since the estimation of the correct value of wake blockage was rather difficult, the overall calculation domain was increased by imposing the requirement on the cube of the velocity at the test section, the wake blockage was not considered in these calculations [17].

$$\varepsilon_{sb} = \frac{1}{4}(D\ H)(W_{domain}\ H_{domain}) \tag{5}$$

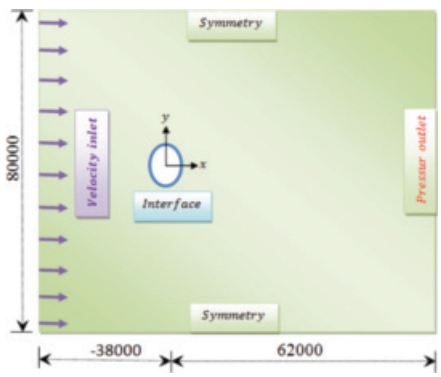

Figure 5: Main dimensions [mm] of the wind Tunnel sub-grid area

$$V_{test\ section} = (1+\varepsilon_{sb})U_{\infty} \tag{6}$$

Two symmetry boundary conditions were used for the two side walls. The circumference around the circular opening centered on the turbine rotational axis was set as an interface, thus ensuring the continuity of the flow field.

The Rotor sub-grid is the fluid area simulating the revolution of the wind turbine and is therefore characterized by a moving mesh, rotating at the same angular velocity of the turbine, whereas the angular velocity of the cylinder depends only on the δ coefficient. Its location coincides exactly with the circular opening inside the Wind Tunnel sub-grid area and is centered on the turbine rotational axis.

Figure 6 shows the main dimensions and the boundary conditions of the Rotor sub-grid area.

In order to obtain faster convergence, it is good engineering practice to provide that the mesh on both sides of the interface (Rotor sub-grid and Wind Tunnel sub-grid areas) has approximately the same characteristic cell size [18].

An isotropic unstructured mesh was chosen for the Rotor subgrid in order to guarantee the same accuracy in the prediction of the rotor's performance during the revolution according to the studies of Commings et al. [19], and also in order to test the prediction capability of a very simple grid. Considering their features of flexibility and adaption capability, unstructured meshes are in fact very easy to obtain, for complex geometries, too, and often represent the "first attempt" in order to get a quick response from the CFD in engineering work.

All blade profiles inside the Rotor sub-grid area were enclosed in a control circle 400 mm in diameter. Unlike the interface, it had no physical significance: its aim was to allow a precise dimensional control of the grid elements in the area close to the rotor blades by adopting a first size function operating from the blade profile to the control circle itself and a second size function operating from the control circle to the whole Rotor sub-grid area, ending with grid elements of the same size of the corresponding Wind tunnel subgrid elements. An interior boundary condition was used for control circle borders thus ensuring the continuity of the cells on both sides of the mesh. A growth factor of 1.2 was set from the surface of the control circle to Rotor sub-grid. Therefore, expanding grid size from 35 mm to 50 mm, as shown in Figure 7.

Two size functions were set inside the control circle, as shown in Figures 7 and 8:

Size function No. 1 started from the control circle to Rotor sub-grid Figure 7.

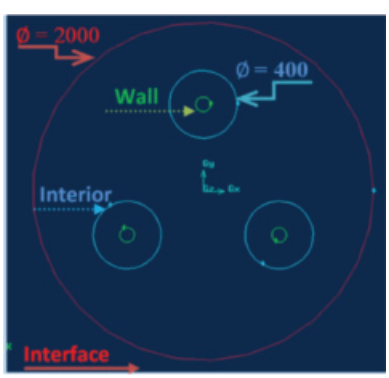

Figure 6: Main dimensions [mm] of the Rotor sub-grid area

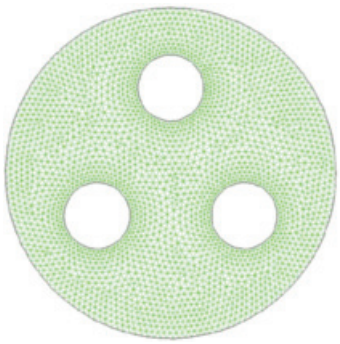

Figure 7: Rotor sub-grid mesh

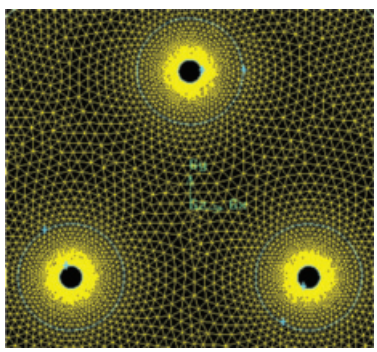

Figure 8: Control circle for cylinder grid mesh section

Size function No. 2 started from the Cylinder profile to the control circle Figure 8.

In order to give better precision to the results, a boundary layer was set in the walls' contour as shown in Figure 9. So, their first row was set to about 0.3 mm and was meshed using 10 rows.

The average torque values, measured in the wind tunnel for a 9 m/s unperturbed wind speed at test section entrance (and different tip speed ratios), were compared with those obtained from CFD analysis for Spalart-Allmaras turbulence model. In this context, the reference [20] described more details about the validation procedure and tests.

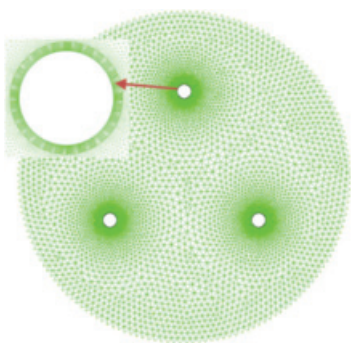

Figure 9: Boundary layer mesh

The optimal grid resolution was selected on the basis of a better distribution of the cylinder y^+ parameter. This parameter is a mesh-dependent dimensionless distance that quantifies the degree of wall layer resolution, in the formula:

$$y^+ = \rho u_t y / \mu \tag{7}$$

Where ρ is air density, u_t is the friction velocity, y the cell distance from the cylinder profile, and μ is the dynamic viscosity.

4. PERFORMANCE AERODYNAMIC MODEL

Determining the wind speed which a wind turbine will operate is the most important step in predicting its performance, and even aids in defining the initial size of it. Once the operating wind speed of the turbine has been decided, the first step in its design is to select an operating tip speed ratio [21] which can be expressed by:

$$TSR = R\ \omega_T / U_\infty \tag{8}$$

The operating speed of the turbine, expressed as Tip Speed Ratios (TSR) shows in Table 2 was set between 1.44 and 3.09. Hence, TSR is defined as:

In the majority of the Darrieus wind turbine research cases, the average power coefficients depend only on the TSR. Accordingly, in this study the results of the DARRIEUS-MAGNUS configuration by using a Fluent digital simulation takes into consideration a new factor which is called λ. The function of the λ defined as:

$$\lambda = R\ \omega_C / U_\infty \tag{9}$$

The final step in predicting the performance of the wind turbine is determining the power it is able to extract from the wind and how efficiently it can accomplish this task. The amount of power the wind turbine is able to draw from the wind is given by:

$$P_{ave} = \omega_T T \tag{10}$$

Therefore, the efficiency of the wind turbine is simply the ratio of the power produced by the wind turbine and the power available in the wind given by the expression:

Table 2: Flow conditions

TSR	***rad/s***	***T*** T_r**/min**	$_T$ ***rad/s*** δ **= 12**
1.44	25.165	240.307	301.980
1.68	29.359	280.357	352.308
2.04	35.650	340.432	427.800
2.33	40.718	388.828	488.616
2.51	43.860	418.832	526.320
2.64	46.135	440.556	553.620
3.09	54.000	515.661	648.000

$$C_{p,\,ave} = \frac{P_T}{P_W} = \frac{P_{ave}}{\frac{1}{2}\,\rho A_s U_\infty^{\,3}} \tag{11}$$

The $C_{p,\,ave}$ equation is significant in this work because it represents a non-dimensional coefficient of performance that is a function of the torque to be used as the objective function for the aerodynamic shape optimization.

We assume that two dimensional airfoil characteristics can be used for the local cylinder element lift and drag coefficients. Care must be taken to use airfoil characteristics appropriate to the wind turbine blade Reynolds number. It is convenient for further calculations to resolve the respective drag and lift coefficients into a normal force coefficient C_N, and a thrust force coefficient C_T as shown in Figure 13.

$$C_N = C_L \cos\theta + C_D \sin\theta \tag{12}$$

$$C_T = C_L \sin\theta - C_D \cos\theta \tag{13}$$

C_N *and* C_T are formulated by these expressions:

$$C_N = \frac{F_N}{1/2\ \rho\ A\ U_\infty^{\,2}} \tag{14}$$

$$C_T = \frac{F_T}{1/2\ \rho\ A\ U_\infty^{\,2}} \tag{15}$$

The thrust coefficient C_T is considered positive when directed forward along the airfoil diameter of the cylinder.

During simulation the reference values are as follows: Area = 1m^2; Density = 2 kg/m^3 and velocity = 1 m/s. According to axes *(x, y)* and to the force *F* we obtain:

$$F_N = F_x\ sin\theta + F_y\ cos\theta \tag{16}$$

$$F_T = F_y\ sin\theta - F_x\ cos\theta \tag{17}$$

Commonly, thrust force, torque and power are expressed in terms of non-dimensional thrust (C_T), torque (C_Q) and power (C_P) coefficients. Where C_P and C_Q satisfy:

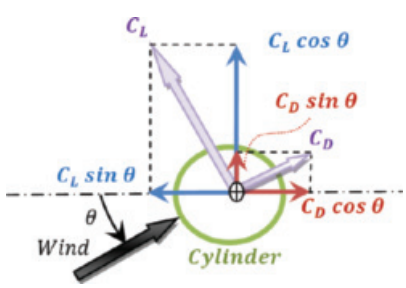

Figure 10: Force coefficients of a cylinder element airfoil

$$C_Q(\theta) = \frac{C_{P,\,ave}}{TSR} = \frac{M(\theta)}{1/2\,\rho\,A\,R\,U_\infty{}^2} \tag{18}$$

$C_Q(\theta)$: Instantaneous torque coefficient.

5. RESULTS AND DISCUSSION

Figure 11 represents the average power coefficient for different values of δ.

In this work three different speeds are obtained: Free wind velocity U_∞, turbine angular velocity ω_T and cylinder rotational speed $_C$. As known, the turbine tip speed ratio depends mainly on the turbine rotational speed; on the other hand, since the originality in this paper is the implementation of MAGNUS Effect, this means a cylinder will have his own rotational speed. Figure 12 shows the evolution of rotor average power coefficient as a function of λ for an incident wind speed of 9 m/s.

As described, the best configuration of this turbine was realized; for this reason, several values of δ were simulated in order to locate the potential zones where the machine gives a wind turbine work. In contrast of the case of a negative torque, this machine can be used to supply a mechanical engine. The Figure 13 shows these zones.

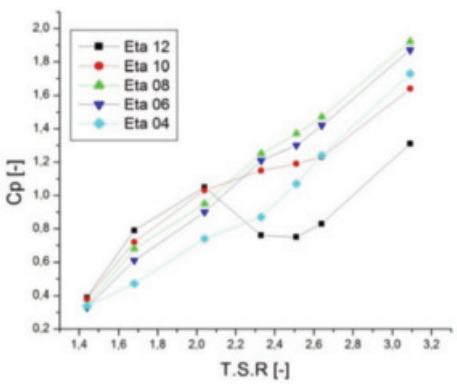

Figure 11: Evolution of rotor average power coefficient as a function of TSR for an incident wind speed of 9 m/s; rotor operation at 5 different δ (*Eta*) values was numerically simulated

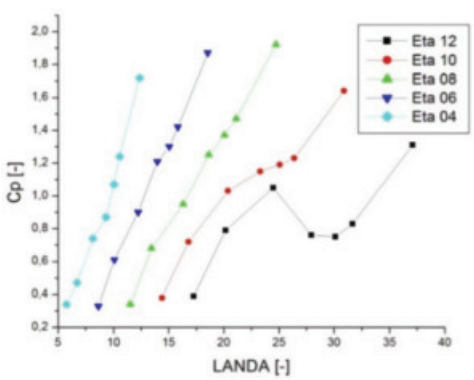

Figure 12: Evolution of rotor average power coefficient as a function of λ (*LANDA*) for an incident wind speed of 9 m/s; rotor operation at 5 different δ (*Eta*) values

It is noted that for δ=10 the machine gives a typical work for wind turbine. Whereas, for $\delta = 4 - 8$ at turbine rotational speed equal to 57.669 rad/s negative torque results were obtained. Figure 14 presents the best wind turbine configuration and shows the average power coefficient according on turbine tip speed ratio for δ=10.

Wind power meteorology has evolved as an applied science, firmly founded on boundary-layer meteorology, but with strong links to climatology and geography. It concerns itself with three main areas: siting of wind turbines, regional wind resource assessment, and short-term prediction of the wind resource. The history, status and perspectives of wind power meteorology are presented, with emphasis on physical considerations and on its practical application. Following a global view of the wind resource, the elements of boundary layer meteorology which are most important for wind energy are reviewed: these elements include wind profiles and shear, turbulence and gust, and extreme winds [22]. The wind speed with 9 m/s is suitable for Algeria, the reason we would like to choose an average annual value of 5 m/s [23]. Figure 15 shows the difference between the evolution of rotor average power coefficient as a function of TSR for an incident wind speeds of 9 m/s and 5 m/s.

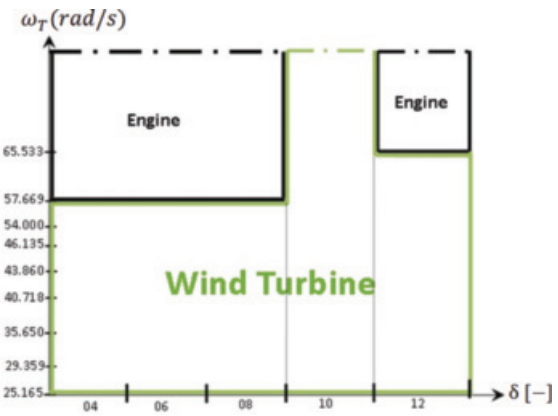

Figure 13: New turbine exploitation zones detection for the zones which is conceived for either wind turbine or mechanical engine works. It depends on various δ values according to several turbine rotational speeds ω_T

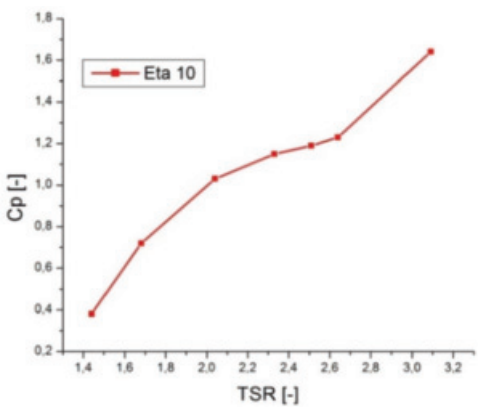

Figure 14: Evolution of rotor average power coefficient as a function of TSR for an incident wind speed of 9 m/s; rotor operation at δ = 10

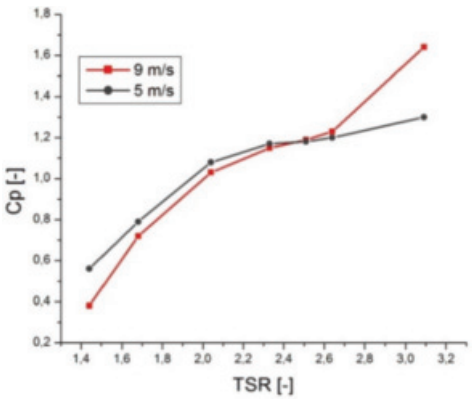

Figure 15: Comparison between evolution of rotor average power coefficient as a function of TSR for an incident wind speeds of 9 m/s and 5m/s; rotor operation at $\delta = 10$

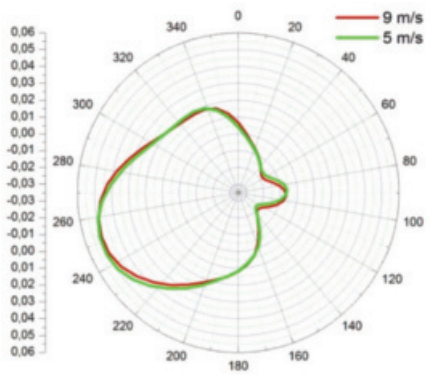

Figure 16: Comparison of the evolution of torque coefficient and of angle of attack as a function of cylinder azimuthal position between two incidents wind speeds of 9 m/s and 5 m/s; TSR 2.33

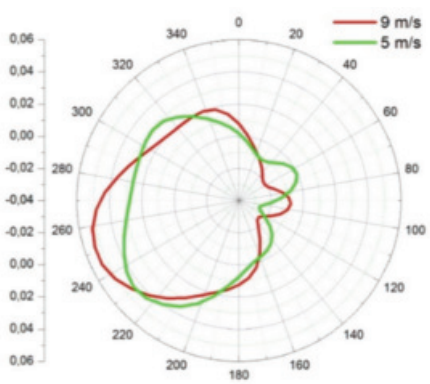

Figure 17: Comparison of the evolution of torque coefficient and of angle of attack as a function of cylinder azimuthal position between two incidents wind speeds of 9 m/s and 5 m/s; TSR 2.51

Figures 16 and 17 show the distribution of the high instantaneous torque coefficient that is only represented in this case. It can be seen that for TSR = 1.44-2.04, the turbine operated at an incident wind speed of 5 m/s and has a torque coefficient higher than that which had operated with 9 m/s; on the other hand, with the TSR = 2.51 the C_Q (U_∞ = 9 m/s) is higher than 5 m/s and finally the torque coefficients are practically similar for TSR = 2.33 and 2.64.

6. CONCLUSIONS

This paper shows the first result of a numerical model based on the application to CFD of the aerodynamic principles for a new approach of a vertical axis DARRIEUS wind turbine on a MAGNUS effect have been presented. The obtained results from the rotor average power coefficient *($C_{P, ave}$)* for any configuration established in this new turbine study are very powerful. The best configuration of this turbine take into account all the dynamic and geometrical characteristics that operate with $\delta = 10$.

The results of a 2-D full campaign of simulations were proposed for a cylinder rotor. Through the analysis of the distribution of the instantaneous torque coefficients and of the relative angles of attack as a function of azimuthal position, two unperturbed wind velocities for computational domain entrance (5 m/s and 9 m/s at $\delta = 10$) were investigated for several values of tip speed ratio, allowing a comparison between their rotor performances.

REFERENCES

[1] Templin, R. J., *Aerodynamic Theory for the NRC Vertical Axis Wind Turbine*, NRC of Canada, Report No, TR LTR-LA-160, 1974.

[2] Strickland, J. H., *The Darrieus Turbine: A Performance Prediction Model Using Multiple Streamtube*, SAND 75–0431.

[3] Oler, J. W., Strickland, J. H., Im, B. J. and Graham, G. H. *Dynamic Stall Regulation of the Darrieus Turbine*, SAND 83–7029.

[4] Allet, A. and Paraschivoiu, I., Viscous Flow and Dynamic Stall Effects on vertical Axis Wind Turbine, *International Journal of Rotating Machine*, 1995, 2(1), pp. 1–14.

[5] Brahimi, M. T., Allet, A. and Praschivoiu, I., Aerodynamic Analysis Models for Vertical Axis Wind Turbine, *International Journal of Rotating Machine*, 1995, 2(1), pp. 15–21.

[6] Masson, C., Leclerc, C. and Praschivoiu, I., Appropriate Dynamic Stall models for Performance Predictions of VAWT With NLF Blades, *International Journal of Rotating Machine*, 1998, 4(2), pp. 129–139.

[7] Praschivoiu, I., *Wind Turbine Design: With Emphasis on Darrieus concept*, 2002, Polytechnic International Press, Montreal.

[8] Mertens, S., Van Kuik, G. and Van Bussel, G., *Performance of a High Tip Speed Ratio H-Darrieus in the skewed Flow on a Roof*, Paper No. aiaa-2003-0523.

[9] Ferreira, S., Bijl, H., Van Bussel, G. and Van Kuik, G., Simulating dynamic stall in a 2D VAWT: modeling strategy, verification and validation with particle image velocimetry data, The Science of making torque from wind, 2007, *Journal of Physics: Conference Series* 75.

[10] Wang, S. and Tao, Z., *Numerical investigation on dynamic stall associated with low Reynolds number flows over airfoils*, Computer Engineering and Technology (ICCET), 2010 2nd International Conference on, Vol. 5.

[11] Kang, C., Zhang, F. and Mao, X., *Comparison study of a vertical-axis spiral rotor and a conventional savonius rotor*, APPEEC 2010 - Proceedings, Art. No. 5448791.

[12] Yaakob, O. B, Tawi, K. B and Sunanto, D. T. S, Computer simulation studies on the effect overlap ratio for savonius type vertical axis marine current turbine, *International Journal of Engineering, Transaction A: Basics*, 2010, 23 (1), pp. 79–88.

[13] Kamoji, M., Kedare, S. and Prabhu, S., Performance tests on helical Savonius rotors, *Renewable Energy*, 2009, 34 (3), pp. 521–529.

[14] Darrieus, G. J. M., *The Darrieus wind turbine*, U.S. Patent Office in 1931.

[15] Moore, D. W., The flow past a rapidly rotating circular cylinder in a uniform stream, *Journal of Fluid Mechanics*, 1957, 2: 541–550.

[16] Castelli, M. R., Englaro, A. and Benini, E., The Darrieus wind turbine: Proposal for a new performance prediction model based on CFD, *Energy*, 2011, 36, 4919–4934.

[17] Castelli, M. R., Englaro, A. and Benini, E., Numerical Analysis of the Influence of Airfoil Asymmetry on VAWT Performance. *Word Academy of Science, Engineering and Technology*, 2012, 61.

[18] Fluent Inc., *Fluent User's Manual*, 2006, pp. 52, 54, 59, 71, 143.

[19] Cummings, R. M., Forsythe, J. R., Morton, S. A. and Squires, K. D. Computational challenges in high angle of attack flow prediction, *Progress in Aerospace Science*, 2003; 39(5): 369–384.

[20] Raciti, Castelli, M, Pavesi, G, Battisti, L, Benini, E. and Ardizzon, G. *Modeling strategy and numerical validation for a Darrieus vertical axis micro-wind turbine*. Vancouver, British Columbia, Canada: ASME 2010.

[21] Cetin, N., Yurdusev, M., Ata, R. and Ozdemir, A., Assessment of optimum tip speed ratio of wind turbines, *Mathematical and Computational Applications*, 2005, Vol. 10, No. 1, pp. 147–154.

[22] Erik, L., Petersen, Niels, G., Mortensen, Lars, L., Jrgen, H. and Helmut, P. F., *Wind Power Meteorology*, RisØ National Laboratory, Roskilde, Denmark. December 1997.

[23] Hammouche, R., *Atlas vent de l'Algérie*, Office National de la Météorologie, Alger 1991.